PHYSICAL REVIEW B **86**, 184113 (2012)

Symmetry of piezoelectric $(1-x)\mathrm{Pb(Mg_{1/3}Nb_{2/3})O_3}$-$x\mathrm{PbTiO_3}$ ($x = 0.31$) single crystal at different length scales in the morphotropic phase boundary region

Kyou-Hyun Kim, David A. Payne, and Jian-Min Zuo[*]
Department of Materials Science and Engineering and Frederick Seitz Materials Research Laboratory, University of Illinois at Urbana-Champaign, Urbana, Illinois 61801, USA

(Received 27 July 2012; revised manuscript received 2 October 2012; published 29 November 2012)

We use probes of three different length scales to examine symmetry of $(1-x)\mathrm{Pb(Mg_{1/3}Nb_{2/3})O_3}$-$x\mathrm{PbTiO_3}$ (PMN-xPT) single crystals in the morphotropic phase boundary (MPB) region at composition $x = 0.31$ (PMN-31% PT). On the macroscopic scale, x-ray diffraction (XRD) shows a mixture of strong and weak diffraction peaks of different widths. The closest match to XRD peak data is made with monoclinic Pm ($\mathrm{M_C}$) symmetry. On the local scale of a few nanometers, convergent beam electron diffraction (CBED) studies, with a 1.6-nm electron probe, reveal no obvious symmetry. These CBED experimental patterns can be approximately matched with simulations based on monoclinic symmetry, which suggests locally distorted monoclinic structure. A monoclinic Cm ($\mathrm{M_A}$ or $\mathrm{M_B}$)-like symmetry could also be obtained from certain regions of the crystal by using a larger electron probe size of several tens of nanometers in diameter. Thus the monoclinic symmetry of single crystal PMN-31%PT is developed only in parts of the crystal by averaging over locally distorted structure on the scale of few tens of nanometers. The macroscopic symmetry observed by XRD is a result of averaging from the local structure in PMN-31%PT single crystal. The lack of local symmetry at a few nanometers scale suggests that the polarization switching results from a change in local displacements, which are not restricted to specific symmetry planes or directions.

DOI: 10.1103/PhysRevB.86.184113 PACS number(s): 77.84.−s, 61.50.Ah, 68.37.Lp, 61.05.J−

I. INTRODUCTION

The symmetry of piezoelectric materials, such as $(1-x)\mathrm{Pb(Mg_{1/3}Nb_{2/3})O_3}$-$x\mathrm{PbTiO_3}$ and $(1-x)\mathrm{Pb(Zn_{1/3}Nb_{2/3})O_3}$-$x\mathrm{PbTiO_3}$ (known as PMN-xPT and PZN-xPT, respectively), has been widely studied for the simple reason that symmetry controls displacements of ionic charge and position, which, in turn, determines directions of spontaneous polarization ($\mathbf{P_S}$) and spontaneous strain ($\boldsymbol{\varepsilon}_\mathbf{S}$), and field ($E$)-induced orientations of ferroelectric and piezoelectric properties. The high-temperature (HT) phase of PMN-xPT and PZN-xPT is cubic $Pm3m$ with no spontaneous distortions. According to published x-T phase diagrams for PMN-xPT and PZN-xPT, the prototypic HT phase spontaneously distorts to rhombohedral (R) $R3m$ symmetry on cooling at low x, or tetragonal (T) $P4mm$ symmetry at higher x, in which $\mathbf{P_S}$ and $\varepsilon_\mathbf{S}$ are constrained to the cubic (noted by the subscript "C") $[111]_\mathrm{C}$ and $[001]_\mathrm{C}$ directions for the R and T phases, respectively. The R and T phases are initially separated by a vertical boundary termed the morphotropic phase boundary (MPB), i.e., a chemically (x)-driven change in morphology.[1,2] The MPB of PMN-xPT and PZN-xPT is defined in a narrow composition region where the R and T phases meet. This phase boundary composition has attracted much attention because displacements maximize as the lattice softens and transforms, giving rise to large enhancements in piezoelectric properties.[3–5]

A large body of work has been reported on the structural origin of the piezoelectric properties for PMN-xPT at the MPB. A new phase with monoclinic (M) symmetry was proposed in the vicinity of MPB[6–10] as identified on pulverized powder samples using x-ray and neutron diffraction studies.[1,2,11] According to the notations proposed by Vanderbilt and Cohen, the monoclinic phase belongs to $\mathrm{M_A}$ or $\mathrm{M_B}$ (Cm) or $\mathrm{M_C}$ (Pm), in which $\mathbf{P_S}$ is aligned along $[uuv]_\mathrm{C}$ ($u > v$) and $[0uv]_\mathrm{C}$ ($u < v$) directions, respectively.[12] The M phase is said to be a structural bridge that facilitates polarization rotation from the R to T phases, which is atypical of ionic displacements. Several research groups, however, have disputed whether the observed M phase truly has the monoclinic symmetry at the local (microscopic) scale.[13–15] The adaptive phase model proposed by Viehland and coworkers states that the M phase found in the MPB region is not a local symmetry but an averaged symmetry obtained from twin-related domain structures.[16] Wang *et al.* from transmission electron microscopy (TEM) studies suggests the monoclinic symmetry is a result of averaging over R or T nanodomains, which supports the adaptive phase model.[17–19] Another point of view, put forward by Kisi *et al.*, suggests the M phase is not a true phase but a distorted structure resulting from residual stress; and the observed M phase is indeed neither sufficient nor necessary for an explanation of the large piezoelectric response in the MPB region.[15] Thus a determination of symmetry, from the local to macroscopic level, in the MPB region, is critical to settle these disputes, and is the purpose of this investigation.

In this study, we selected a PMN-31%PT single crystal for symmetry determinations, which is an established MPB composition with reported properties.[20] Previously, the symmetry of PMN-xPT was investigated by optical microscopy, high-resolution XRD, and neutron diffraction.[6–9] PMN-xPT, however, is known for having complex hierarchical domain structures, starting from nanodomains (of a few, to tens of nanometers), to microdomains (of tenths, to tens of microns). The symmetry determination of nanodomains, therefore, requires a small diameter probe with nanometer resolution in order to determine the local symmetry. Considering this limitation, CBED performed in a TEM is an appropriate tool for a determination of local symmetry.[21–25] The rocking

©2012 American Physical Society

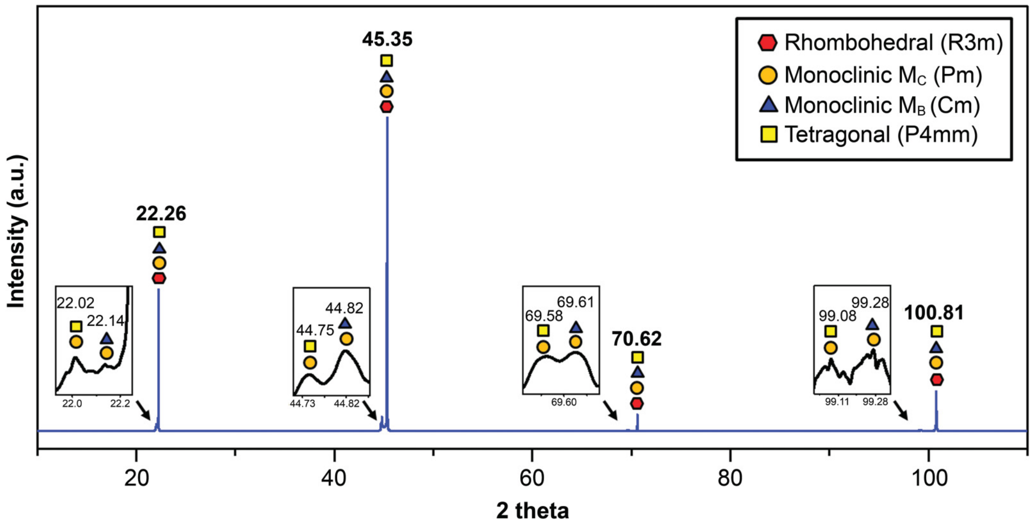

FIG. 1. (Color online) 2θ XRD data obtained from annealed PMN-31%PT. The same crystal was studied by electron diffraction. The diffraction peaks are labeled by numbers and indexed with symbols for different structures listed in the figure legend.

curve information recorded in the CBED patterns is very sensitive to the symmetry of the crystal structure.[26–28] Local symmetry within a few nanometers can be studied with a field emission gun, which can provide electron probes of ~2 nm in diameter or less. The symmetry over several tens of nanometers can be investigated with a thermionic electron source, which forms a larger probe size of tens of nanometers. Previous symmetry studies were performed on powders or ion-milled specimens.[7–10,17–19,29] However, the domain structure of PMN-xPT is very sensitive to specimen history, especially, applied and residual stresses, electric poling and heat-treatment conditions.[30] In this study, all specimens were annealed to attain the original structure in order to minimize the effects of stresses induced by polishing and ion-milling.[30] The symmetry of PMN-31%PT single crystal was then determined from CBED patterns obtained along several zone axes, and by comparison with electron diffraction simulations. In addition, a recently proposed algorithm was used to quantify the symmetry recorded in the experimental CBED patterns through use of a cross-correlation coefficient.[31] The physical insight will be useful for an understanding of the structure-property relations of the piezoelectric crystals.

II. EXPERIMENTAL

PMN-31%PT specimens were selected from a melt-grown crystal, which had been sliced normal to the four principal orientations, $[001]_C$, $[010]_C$, $[011]_C$, and $[111]_C$, and thinned to less than 40 μm by mechanical polishing. Details of the specimen preparation are reported elsewhere.[30] An Ar-ion beam (4.5 kV, 6° incidence) was used to mill the specimens for perforation and electron transparency (Precision Ion Polishing System, PIPS^{TM}, Gatan, USA). It is known that ion-milling induces artificial domain structures in piezoelectric materials from surface stress, and so specimens were annealed at 500 °C in air with slow cooling. After annealing, XRD (PANalytical X'pert MRD system, Philips) was used to determine lattice

TABLE I. Measured and calculated 2θ angles and their differences. The calculation is based on the reported crystal structures of PMN-xPT.[9,10,34] The composition (x) of the referenced crystal structure is specified in the table.

Exp. ($x = 0.31$)	*R3m* ($x = 0.09$)			*Cm* ($x = 0.29$)			*Pm* ($x = 0.32$)			*P4mm* ($x = 0.39$)		
2θ	(h, k, l)	2θ	$\Delta 2\theta$ (deg)	(h, k, l)	2θ	$\Delta 2\theta$ (deg)	(h, k, l)	2θ	$\Delta 2\theta$ (deg)	(h, k, l)	2θ	$\Delta 2\theta$ (deg)
22.02				–	–	–	001	22.04	0.02	001	21.92	−0.1
~22.14	–	–	–	110	22.07	−0.07	100	22.10	−0.04	–	–	–
22.26*	001	22.08	−0.18	001	22.12	−0.14	010	22.17	−0.09	100	22.26	0
44.75	–	–	–	–	–	–	002	44.96	0.21	002	44.70	−0.05
44.82				220	45.02	0.2	200	45.07	0.25	–	–	–
45.35*	002	45.04	−0.31	002	45.12	−0.23	020	45.26	−0.09	200	45.41	0.06
69.58	–	–	–	–	–	–	003	70.00	0.42	003	69.56	−0.02
69.61	–	–	–	330	70.14	0.53	300	70.18	0.57	–	–	–
70.62*	003	70.12	−0.5	003	70.27	−0.35	030	70.46	−0.16	300	70.75	0.13
~99.08	–	–	–	–	–	–	004	99.77	0.69	004	99.02	−0.06
~99.28	–	–	–	440	100.01	0.73	400	100.08	0.8	–	–	–
100.81*	004	99.98	−0.83	004	100.23	−0.58	040	100.55	−0.26	400	101.04	0.33

*An asterisk indicates strong peaks observed in the experimental XRD.

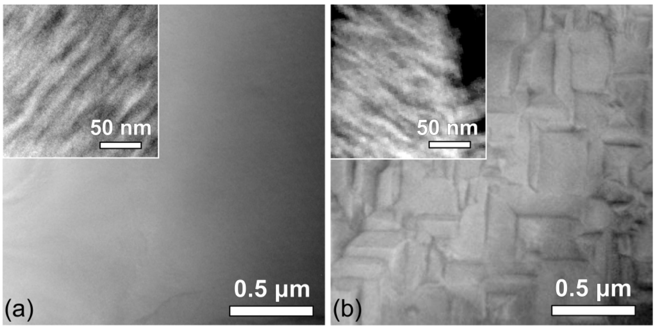

FIG. 2. Bright-field images recorded from (a) the annealed PMN-31%PT crystal and (b) after ion milling. The image in (a) shows uniform contrast at medium magnification while the image in (b) shows submicron domain structure. The insets in (a) and (b) are for high magnification showing nandomains of ~10 nm in width in PMN-31%PT.

parameters before TEM studies with two different beam sizes. Selected area electron diffraction (SAED or spot patterns) and CBED patterns were recorded along the zone axes of $[001]_C$, $[011]_C$, and $[111]_C$, respectively. We used a focused beam of 1.6 nm in FWHM (Full-Width Half-Maximum) in JEOL 2010F-FEG, and 35 nm in JEOL 2100 LaB_6, for the CBED studies. As mentioned, symmetry obtained with the smaller 1.6-nm beam will be referred to as local symmetry, whereas, symmetry obtained with the 35-nm probe will be termed the averaged symmetry obtained over multiple nanodomains. We also recorded SAED spot patterns, which were indexed on reported crystallographic data.

For the symmetry determination, CBED patterns were recorded from different areas of the specimen in numbers ranging from tens to hundreds in an effort to search for the highest symmetry. Theoretical CBED patterns were then simulated based on diffraction pattern indexing, and compared with the experimental CBED results, for a determination of crystal symmetry. The symmetry recorded in the CBED patterns was quantified through use of a cross-correlation coefficient (γ):

$$\gamma = \frac{\sum_{x,y}\{[I_A(x,y)-\overline{I_A}]\cdot[I_B(x,y)-\overline{I_B}]\}}{\sqrt{\{\sum_{x,y}[I_A(x,y)-\overline{I_A}]^2\}\cdot\{\sum_{x,y}[I_B(x,y)-\overline{I_B}]^2\}}},$$

where $I_{A\,\mathrm{or}\,B}(x,y)$ and $\bar{I}_{A\,\mathrm{or}\,B}(x,y)$ are the intensity of two symmetry related CBED discs A (or B) at (x, y) and a mean value of the template A (or B), respectively. The symmetry can be quantified for the rotational and mirror symmetry elements, and γ has the maximum value of 100% for theoretical patterns when the patterns are perfectly symmetrical. For experimental CBED patterns, the symmetry quantification was calibrated using a Si single crystal. For the perfect symmetry in experimental CBED patterns, the γ values ranged from 98–99% with a standard deviation of ~3%. Details for the symmetry quantification are explained elsewhere.[31]

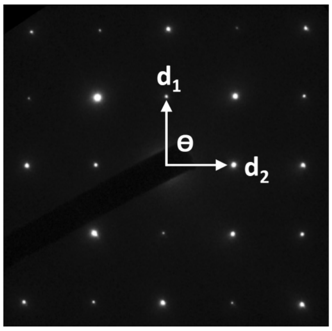

d	nm^{-1}	Error
d_1	2.421	± 0.016 nm^{-1}
d_2	2.439	
d_2/d_1	1.007	-1.27 ~ 1.37% (0.994 ~ 1.021)
θ	~ 90°	

FIG. 3. Selected area electron diffraction pattern recorded along $[001]_C$.

III. CRYSTAL STRUCTURE AND ELECTRON DIFFRACTION SIMULATION

Several crystal structures have been reported for PMN-xPT[8,32–34] depending on x and T. Slodczyk *et al.*[35] reported a R structure with $R3m$ symmetry for $x = 0.09$ and $T = 12$ K. The lattice parameters were $a = b = c = 4.0364$ Å, and $\alpha = 89.8826°$, and with positional coordinates Pb (0, 0, 0), Ti/Nb/Mg (0.534, 0.534, 0.534), and O (0.541, 0.541, 0.03). These data were obtained by powder XRD. Here, we use rhombohedral axes, rather than hexagonal axes (used by others), for a direct comparison between orthogonal axes and structural models.

The reported M structures of PMN-xPT belong to two different space groups of monoclinic symmetry, according to the notation of Vanderbilt and Cohen.[12] M_B (or M_A) belongs to space group Cm with lattice parameters $a = 5.6951$ Å, $b = 5.6813$ Å, $c = 4.0138$ Å, and $\beta = 90.136°$, and positional coordinates Pb (0, 0, 0), Ti/Nb/Mg (0.5250, 0, 0.498), O_1 (0.54, 0, −0.01), and O_2 (0.317, 0.267, 0.48). M_C belongs to space group of Pm with lattice parameters $a = 4.0183$ Å, $b = 4.0046$ Å, $c = 4.0276$ Å and $\beta = 90.146°$, and positional coordinates Pb (0, 0, 0), Ti/Nb/Mg (0.509, 0.50, 0.5479), O_1 (0.47, 0, 0.57), O_2 (0.417, 0.5, 0.059), and O_3 (−0.02, 0.5, 0.57). These data for Cm (M_A or M_B) and Pm (M_C) symmetry were obtained by powder XRD for $x = 0.29$ and 0.32, respectively, at room temperature.[9]

TABLE II. Observable symmetry in CBED in the zero-order Laue zone (ZOLZ) for the reported crystal structures of PMN-PT and their space group (SG) and point group (PG).

			Symmetry in the zero-order Laue zone						
Crystal Structure	SG	PG	[001]	[010]	[100]	[011]	[101]	[110]	[111]
R	*R3m*	*3m*	*m*	*m*	*m*	*m*	*m*	*1*	*3m*
T	*P4mm*	*4mm*	*4mm*	*m*	*m*	*m*	*m*	*m*	*m*
M_B	*Cm*	*m*	*m*	*1*	*m*	*1*	*m*	*1*	*1*
M_C	*Pm*	*m*	*m*	*1*	*m*	*1*	*m*	*1*	*1*

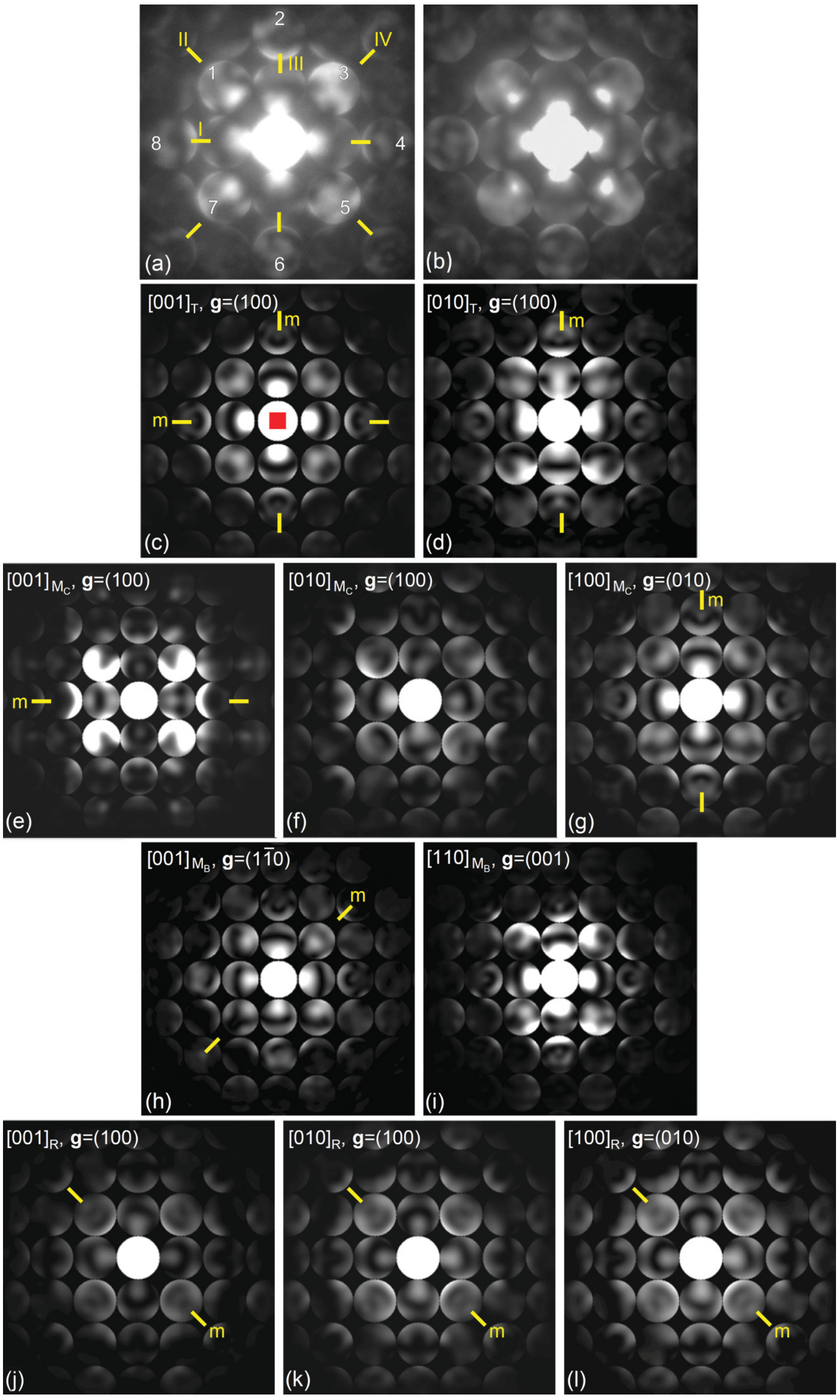

FIG. 4. (Color online) Experimental CBED patterns recorded along (a) $[001]_C$ and (b) $[010]_C$ and (c)–(l) simulated CBED patterns based on electron diffraction indexing results. The **g** refers to the first reflection along the horizontal direction.

Singh *et al.* reported a T structure with space group *P4mm* for $x = 0.39$ at room temperature. The lattice parameters were $a = 3.9920$ Å and $c = 4.0516$ Å at $x = 0.39$, and positional coordinates Pb (0, 0, 0), Ti/Nb/Mg (0.5, 0.5, 0.532), O_1 (0.5, 0.5, 0.054), and O_2 (0.5, 0, 0.601).[9]

All the electron diffraction simulations here use the above reported crystal structures, the atomic scattering factors of Doyle and Turner,[36] and the absorption parameters of Bird and King.[36,37] The cation substitutions were treated as random, and the occupancy factors for Mg/Nb/Ti were calculated as 0.23, 0.46, and 0.31, respectively, for $x = 0.31$.

IV. RESULTS

A. X-ray diffraction from the $[001]_C$ oriented PMN-31%PT single crystal

Figure 1 shows 2θ scan by x-ray obtained from an annealed crystal, which was later used in TEM studies. The diffraction pattern consists of strong diffraction peaks accompanied by a number of very weak diffraction peaks. The strong diffraction peaks and their sharpness indicate the quality of the annealed crystal. The high intensity peaks have 2θ values of 22.26°, 45.35°, 70.62°, and 100.81°. The weak peaks are clearly

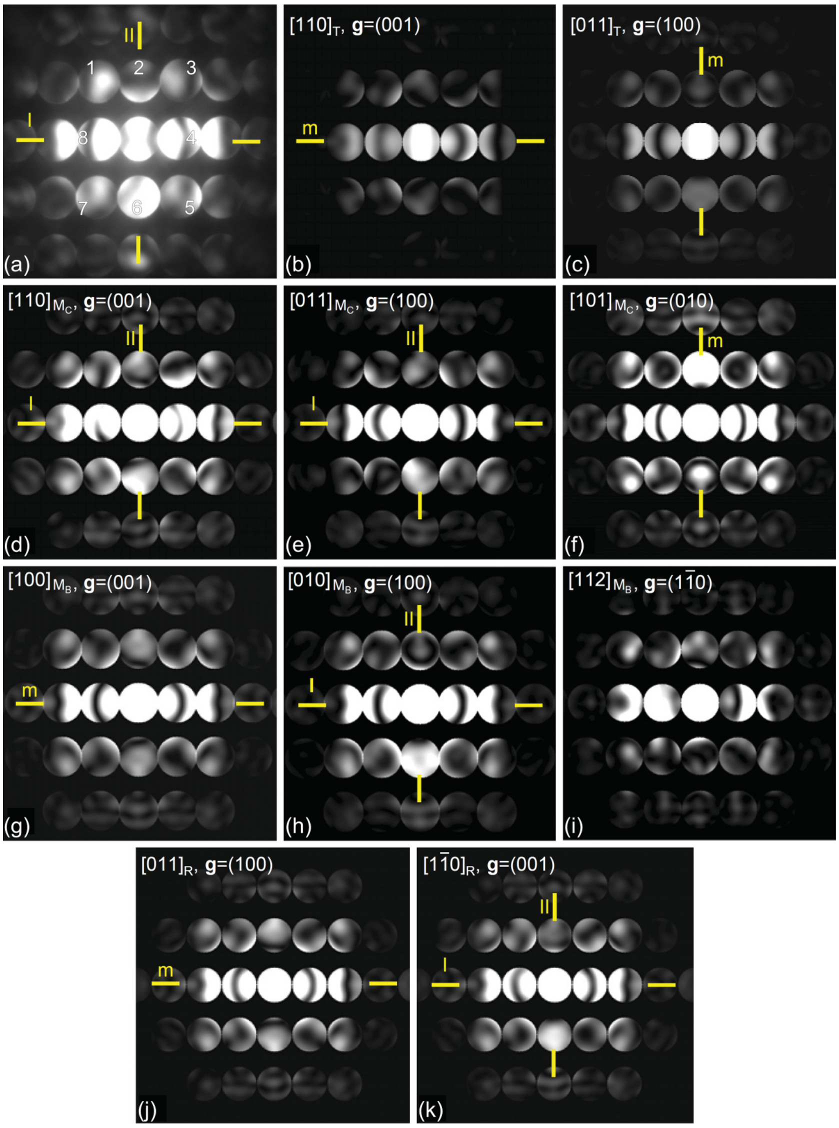

FIG. 5. (Color online) (a) Experimental CBED pattern recorded along $[011]_C$ and (b)–(k) simulated CBED patterns based on the electron diffraction indexing results. The **g** refers to the first reflection along the horizontal direction.

separated, as highlighted by the insets in Fig. 1, at 2θ values of $\sim 22^\circ$, $\sim 44^\circ$, $\sim 69^\circ$, and $\sim 99^\circ$. The FWHM of the strong diffraction peaks is about 0.02°, which is close to the instrument resolution of 0.013° in 2θ. The weak diffraction peaks are significantly broader (5 times) than the strong diffraction peaks. Our 2θ values are compared with values calculated from the literature in Sec. III (see Table I). Calculations are for a variety of compositions with different x values (see above), but the compositions of the reported M_B ($x = 0.29$) and M_C ($x = 0.32$) are close to PMN-31%PT. Our single crystal XRD data was then indexed with all referenced structures and marked as shown in Fig. 1. Table I summarizes the indexing results. The M_C structure could be indexed on all the diffraction peaks in the experimental XRD data. Nevertheless, the average structure for PMN-31%PT cannot be determined unambiguously from the XRD data alone and is a topic of our TEM studies that follow.

B. Symmetry determination at several nanometers scale

Our symmetry determinations were carried out on annealed specimens, which are closest to the structure of unpoled PMN-31%PT single crystal. A typical bright-field (BF) image of annealed PMN-31%PT is given in Fig. 2(a). This image has similar contrast and is comprised of fine nanodomains as illustrated in the inset of Fig. 2(a). A BF image of the ion-milled sample is given in Fig. 2(b). By comparison, the ion-milled sample consists of microdomains with widths of a few tenths of microns. Nevertheless, the individual microdomains in Fig. 2(b) are also comprised of nanodomains, as reported previously.[30]

For the selection of the optimum combinations of zone axis patterns (ZAPs) necessary for symmetry determinations, we compared the space group, point group, and corresponding zone-axis symmetry of the diffraction group[21] for each proposed structural model of PMN-xPT, as listed in Table II. Each zone axis has the distinguished symmetry in the ZOLZ CBED pattern. To make use of Table II, we first investigated the sample orientations of $[001]_C$ and $[010]_C$. The symmetry of PMN-31%PT single crystals will be determined by following ZAPs from $[001]_C$ to $[111]_C$ with the help of CBED simulations.

The focused beam probe of 1.6 nm in FWHM was used to investigate the local symmetry. What follows is an account of comparison between experimental CBED patterns recorded using this small probe and simulations. We show that experimental patterns contain no obvious symmetry and they can be approximately matched with simulations based on the monoclinic symmetry.

1. Local symmetry along $[001]_{\mathrm{C}}$ *and* $[010]_{\mathrm{C}}$

Figure 3 shows the spot diffraction pattern obtained along zone axis $[001]_{\mathrm{C}}$. The recorded diffraction pattern was indexed with the reported structures of PMN-xPT. The spot patterns consist of sharp and single crystal diffraction peaks without any peak splitting or additional diffraction peaks. According to the reported phase diagram of PMN-xPT, $x = 0.31$ lies within the MPB region.[8] Diffraction pattern indexing was carried out on all possible crystal structures considering the experimental error. For example, the spot diffraction pattern of Fig. 3 can be indexed as the zone axes of $[001]_{\mathrm{T}}/[010]_{\mathrm{T}}$, $[001]_{\mathrm{M_C}}/[010]_{\mathrm{M_C}}/[100]_{\mathrm{M_C}}$, $[001]_{\mathrm{M_B}}/[110]_{\mathrm{M_B}}$ and $[001]_{\mathrm{R}}/[010]_{\mathrm{R}}/[100]_{\mathrm{R}}$. These indexing results are considered for the CBED simulations.

Figures 4(a) and 4(b) show two examples of experimental CBED patterns recorded from $[001]_{\mathrm{C}}$ and $[010]_{\mathrm{C}}$ zone axes. We quantified the amount of mirror symmetry in the recorded CBED patterns in four directions that are marked as I, II, III, and IV in Fig. 4(a). Quantification was based on cross correlations between pairs of diffraction discs expected to have mirror symmetry.[31] For example, a mirror along I was quantified for Figs. 4(a) and 4(b) using the disc pairs of 1/7, 2/6, and 3/5 [for labeling, see Fig. 4(a)]. Similar procedures were carried out for possible mirror symmetry along II, III, or IV. The highest cross-correlation coefficient (γ) was detected along direction I, i.e., $\gamma_{\mathrm{m(I)}} = 42\%$ (the subscript “m” with the parentheses “()” indicates the mirror quantification along the direction in parentheses) for the $[100]_{\mathrm{C}}$ pattern. The $[010]_{\mathrm{C}}$ pattern gave $\gamma_{\mathrm{m(II)}} = 57\%$ along direction II. For reference, a perfect mirror symmetry quantified for single crystal silicon gave γ_{m} values between 98% and 99% with a variation of $\sim 3\%$.[31] Based on the low cross-correlation coefficients, the experimental CBED patterns show trivial, 1-fold rotation symmetry, along $[001]_{\mathrm{C}}$ and $[010]_{\mathrm{C}}$.

The CBED patterns were then simulated for different thicknesses (t) based on the indexing determinations. The simulation results are best matched to the experimental patterns at $t \sim 50$ nm. The simulated CBED patterns based on the different structural models are shown in Figs. 4(c)–4(l). Now, the observed symmetry in the experimental CBED pattern is compared with simulation results. In Fig. 4(c), the pattern symmetry of the T structure is 4mm along zone axis $[001]_{\mathrm{T}}$. The simulation results for $[010]_{\mathrm{T}}$, $[001]_{\mathrm{M_C}}/[100]_{\mathrm{M_C}}$, $[001]_{\mathrm{M_B}}$, and $[001]_{\mathrm{R}}/[010]_{\mathrm{R}}/[100]_{\mathrm{R}}$ CBED patterns have the mirror (m) symmetry element. No such mirror element was observed in the simulation patterns for $[010]_{\mathrm{M_C}}$ and $[110]_{\mathrm{M_B}}$ similar to the experimental CBED patterns. Based on the experimental and simulation results here, therefore, the closest matches with experiment are $[010]_{\mathrm{M_C}}$ and $[110]_{\mathrm{M_B}}$.

2. Local symmetry along $[011]_{\mathrm{C}}$

Figure 5(a) shows a selected experimental CBED pattern for ZOLZ along zone axis $[011]_{\mathrm{C}}$. The $[011]_{\mathrm{C}}$ CBED patterns were measured for two possible mirror orientations along lines I and II in Fig. 5(a). The highest cross-correlation coefficient for mirror symmetry was obtained for line II with $\gamma_{\mathrm{m(II)}} = 59\%$.

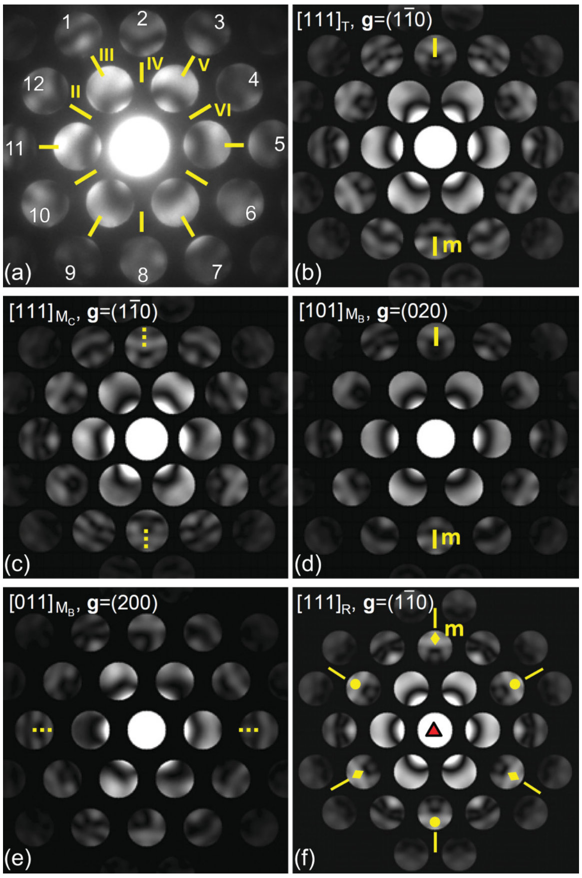

FIG. 6. (Color online) (a) Experimental CBED pattern and (b)–(f) simulated CBED patterns for the selected crystal structures. The **g** refers to the first reflection along the horizontal direction.

Figures 5(b)–5(k) show the simulated CBED patterns corresponding to the indexing results. Based on the simulations, several indexing options can be directly excluded from possible solution for the $[011]_{\mathrm{C}}$ zone axis. The simulated patterns for $[110]_{\mathrm{T}}/[011]_{\mathrm{T}}$, $[101]_{\mathrm{M_C}}$, $[100]_{\mathrm{M_B}}$, and $[011]_{\mathrm{R}}$ have mirror symmetry, which is inconsistent with the low cross-correlation coefficient obtained from experimental data. The simulated CBED pattern for $[112]_{\mathrm{M_B}}$ is obviously different from the experimental pattern as shown in Fig. 5(i). Patterns for $[110]_{\mathrm{M_C}}/[011]_{\mathrm{M_C}}$, $[010]_{\mathrm{M_B}}$ and $[1\bar{1}0]_{\mathrm{R}}$ show no mirror symmetry like the experimental pattern. The amount of deviation from mirror symmetry in these simulated patterns was then measured along I and II in the same way as done previously for the experimental patterns. According to these measurements, $[110]_{\mathrm{M_C}}$ is more mirror symmetrical along line I [$\gamma_{\mathrm{m(I)}} = 60\%$] compared with line II [$\gamma_{\mathrm{m(II)}} = 38\%$], which is inconsistent with the experimental pattern. For $[011]_{\mathrm{M_C}}$, significant breakdown for mirror symmetry occurred along lines I and II [$\gamma_{\mathrm{m(I,II)}} < 30\%$]. Simulated patterns for $[010]_{\mathrm{M_B}}$ [$\gamma_{\mathrm{m(I)}} = 16\%$, $\gamma_{\mathrm{m(II)}} = 88\%$] and $[1\bar{1}0]_{\mathrm{R}}$ [$\gamma_{\mathrm{m(I)}} = 33\%$, $\gamma_{\mathrm{m(II)}} = 72\%$] are more mirror-symmetrical along line II in agreement with experimental data. Based

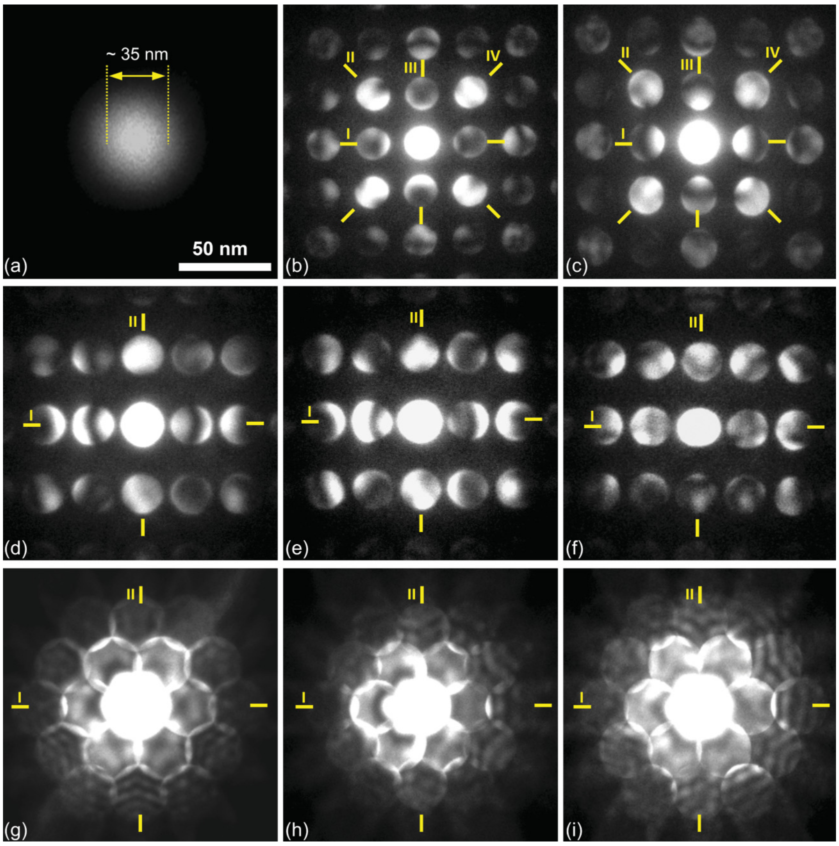

FIG. 7. (Color online) Selected CBED patterns recorded using the larger electron probe size of ∼35 nm. The probe diameter is shown in (a). The experimental CBED patterns are shown for zone axes (b) and (c) $[001]_C$, (d)–(f) $[011]_C$, and (g)–(i) $[111]_C$. Mirror symmetry is quantified along the lines indicated in the CBED patterns.

on these results, the possible matches here are for $[010]_{M_B}$ and $[1\bar{1}0]_R$.

3. *Local symmetry along [111]*$_C$

Figure 6(a) shows an experimental CBED pattern recorded along zone axis $[111]_C$, in which the first-order diffraction discs show 6-fold like features, but with significant symmetry breakdown in all discs. The breakdown is even more significant in the second- and third-order diffraction discs. The amount of mirror symmetry was quantified by using the second- and third-order discs along the 8 possible mirror directions indicated in Fig. 6(a). The largest γ_m value is 26%, indicating a lack of symmetry, except for a trivial 1-fold rotation axis.

Figures 6(b)–6(f) are the simulated CBED patterns (t = 60 nm) corresponding to the indexing results for the $[111]_C$ zone axis. The $[111]_T$, $[101]_{M_B}$, and $[111]_R$ show higher symmetry than the experimental patterns and they are thus excluded from possible solutions for the zone axis of $[111]_C$. For further comparison, we quantified the mirror symmetry for $[111]_{M_C}$ and $[011]_{M_B}$ along the dotted line indicated, and the γ_m values were found to be 73% for $[111]_{M_C}$, and 95% for $[011]_{M_B}$, respectively. These γ_m values calculated from the simulations were significantly higher than those obtained from the experimental CBED pattern (<26%).

C. Symmetry determination at tens of nanometers scale

The symmetry of CBED patterns was also investigated by using a larger electron probe of 35 nm [see Fig. 7(a)]. Based on the characteristic 10-nm size of nanodomains (see Fig. 2), the probe shown in Fig. 7(a) would cover multiple nanodomains.[38–40] CBED patterns were obtained from different regions of the crystal along $[001]_C$, $[011]_C$, and $[111]_C$ zone axes. Figures 7(b)–7(i) show selected experimental CBED patterns recorded along zone axes $[001]_C$, $[011]_C$, and $[111]_C$. The γ values for mirror symmetry were determined along the orientations indicated. The symmetry quantification results are summarized in Table III. The lowest and highest γ_m values measured from multiple CBED patterns are shown in the table. The experimental CBED patterns showing the maximum γ_m values were used for the symmetry determination.

For $[001]_C$, Figs. 7(b) and 7(c) show two selected patterns from different regions of the PMN-31%PT crystal. Figure 9(b) has the highest γ_m value of ∼85% along line IV, while the other directions were less, 40% ∼ 55%. For the second CBED pattern shown in Fig. 7(c), the calculated γ_m values ranged from 10% to 57%.

The CBED patterns recorded along $[011]_C$ [see Figs. 7(d)–7(f)] show different extents of possible mirror symmetry. Based on quantification results, the recorded patterns can be categorized into three categories. The first type [see Fig. 7(d)] has a higher cross-correlation coefficient along line II [$\gamma_{m(II)}$ = 54%] than for line I [$\gamma_{m(I)}$ = 36%]. The second type [see Fig. 7(e)] is greater along line I [$\gamma_{m(I)}$ = 58%] than for line II [$\gamma_{m(II)}$ = 38%]. The third type [see Fig. 7(f)] has lower values of 36% and 32%, for lines I and II, respectively.

We also observed three types of CBED patterns for the $[111]_C$ direction as shown in Figs. 7(g), 7(h), and 7(i). The experimental CBED patterns have no *3m* symmetry, so the R structure is directly ruled out. As listed in Table III, the first type [see Fig. 7(g)] has the highest cross-correlation coefficient for mirror symmetry along line II [$\gamma_{m(II)}$ = 83%], while the second type [see Fig. 7(h)] has the highest value along line

TABLE III. Mirror quantification for $[001]_C$, $[011]_C$ and $[111]_C$ CBED patterns obtained with a probe size of 35 nm in diameter and comparison with simulated CBED patterns for M_B (Cm) symmetry. (The simulations are indicated by parentheses.)

			γ_m (%)		
			Exp.		M_B (Cm)
Zone axis	CBED pattern	Mirror direction	low	high	(Cal.)
$[001]_C$	Fig. 7(b) ($[001]M_B$, Fig. 8(a))	I	31	40	36
		II	43	55	19
		III	28	53	27
		IV	74	85	100
	Fig. 7(c) ($[110]M_B$, Fig. 8(b))	I	15	10	35
		II	20	21	37
		III	45	57	41
		IV	12	41	0
$[001]_C$	Fig. 7(d) ($[010]M_B$, Fig. 8(c))	I	33	36	29
		II	52	54	84
	Fig. 7(e) ($[112]M_B$, Fig. 8(d))	I	52	58	61
		II	9	38	20
	Fig. 7(f)	I	36		–
		II	32		–
$[111]_C$	Fig. 7(g) ($[101]M_B$, Fig. 8(e))	I	22	27	13
		II	78	83	100
	Fig. 7(h) ($[011]M_B$, Fig. 8(f))	I	69	77	96
		II	40	39	13
	Fig. 7(i)	I	39		–
		II	53		–

I [$\gamma_{m(I)} = 77\%$]. The results for the third type [see Fig. 7(i)] were significantly lower.

From the simulated patterns for $[001]_C$, $[011]_C$, and $[111]_C$ as described in Sec. IV B, the Cm (M_B) symmetry provided the closest match with the zone axes investigated here. Figure 8 summarizes the results for CBED simulations based on Cm symmetry. For example, the simulated patterns in Figs. 8(a)–8(f) are in close match with the experimental patterns shown in Figs. 7(b)–7(h), respectively. The approximate mirror observed in Fig. 7(b) is consistent with the mirror element found in $[001]_{M_B}$ [see Fig. 8(a)]. The $[001]_C$ CBED pattern shown in Fig. 7(c) is comparable with $[110]_{M_B}$ shown in Fig. 8(b). For $[011]_C$, the $[010]_{M_B}$ and the $[112]_{M_B}$ simulations are in agreement with the experimental data given in Figs. 7(d) and 7(e), respectively. $[010]_{M_B}$ has a higher cross-correlation coefficient for more mirror-like symmetry along line II [$\gamma_{m(I)} = 29\%$, $\gamma_{m(II)} = 84\%$], and $[112]_{M_B}$ is more mirror-symmetrical along line I [$\gamma_{m(I)} = 61\%$, $\gamma_{m(II)} = 20\%$]. For $[111]_C$, $[101]_{M_B}$ has perfect mirror symmetry while $[011]_{M_B}$ has approximate mirror about the dotted line with a γ_m value of 96%. The two selected $[111]_C$ CBED patterns in Figs. 7(g) and 7(h) are thus comparable with $[101]_{M_B}$ and $[011]_{M_B}$, respectively.

V. DISCUSSION

XRD determines the average symmetry at the length scale of x-ray coherence (hundreds of nanometers). From the XRD result, the strong peaks are for dominant, averaged, domain orientations, whereas the weak peaks are from domains of different orientations. Results for XRD indexing of single crystal data in Table I are close to monoclinic M_C (Pm) symmetry. Evidence of lattice differences with the reported data is observed in the strong diffraction peak positions. The experimental peak positions deviate slightly from the calculated peak positions by 0.07° ~ 0.3°. The difference in the peak positions is 0.15 ~ 0.2%. Overall, the XRD results suggest the PMN-31%PT crystal has monoclinic M_C structure with small lattice distortions from published data based on powder specimens.[9]

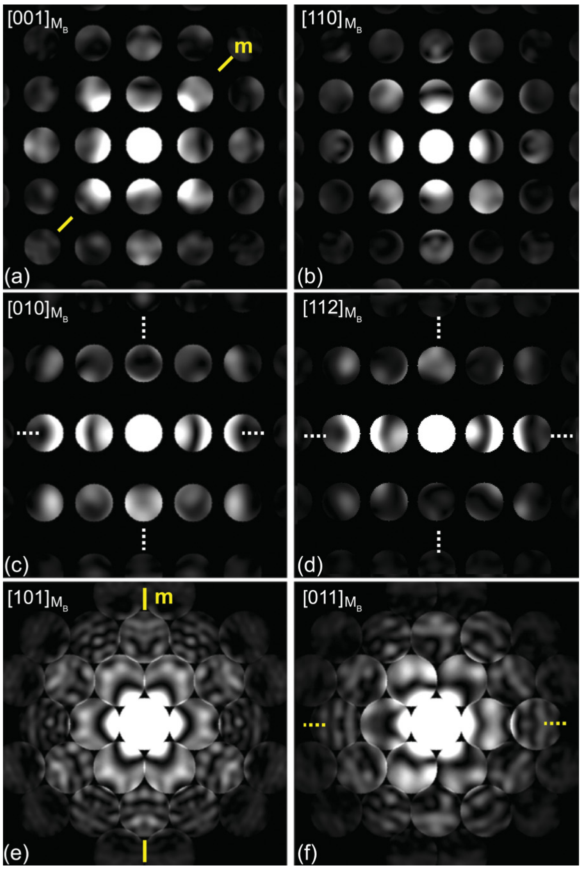

FIG. 8. (Color online) Simulated CBED patterns based on the structure of the M_B phase for zone axes (a) [001], (b) [110], (c) [010], (d) [112], (e) [101], and (f) [011].

Approximate mirror symmetries were detected when probing with the larger 35-nm diameter electron beam. The experimental CBED patterns, with help of simulations, can be indexed with the Cm symmetry as shown in Sec. IV C. However, the observed mirror symmetry in the experimental pattern is imperfect with the highest cross-correlation coefficients of $\gamma_m = 83 \sim 85\%$ compared with γ_m values of 96 to 100% for simulated patterns. Experimentally, we found that the mirror symmetry can be detected using a 15 nm, or larger, sized electron probe. The 35-nm probe used here is twice as larger than required for detecting the mirror symmetry element. Thus the averaged symmetry at 35-nm length scale is therefore concluded as a monoclinic Cm-like symmetry.

By comparison, when using the smaller 1.6 nm beam size, the cross-correlations for mirror symmetry are significantly less in the range of 0 ~ 42%, 10 ~ 66%, 8 ~ 59% and

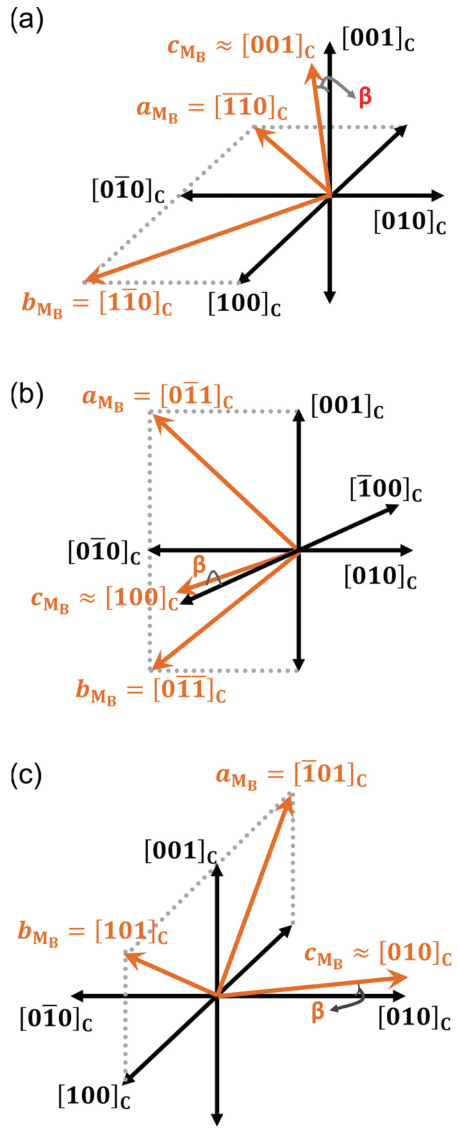

FIG. 9. (Color online) Orientation relationships between monoclinic $\mathrm{M_B}$ (Cm) and pseudocubic axes.

$0 \sim 26\%$ for CBED patterns recorded along zone axes $[001]_{\mathrm{C}}$, $[010]_{\mathrm{C}}$, $[011]_{\mathrm{C}}$, and $[111]_{\mathrm{C}}$ respectively. These experimental CBED patterns resolve trivial symmetry of 1-fold rotation for all investigated zone axes. In the simulated CBED patterns, the monoclinic $\mathrm{M_B}$ and $\mathrm{M_C}$ predict different mirror symmetry along $[001]_{\mathrm{C}}$, $[010]_{\mathrm{C}}$, $[011]_{\mathrm{C}}$, and $[111]_{\mathrm{C}}$, dependent on the orientation of the monoclinic axes. For example, the experimental $[010]_{\mathrm{C}}$ CBED pattern is expected to have either the symmetry of $[001]_{\mathrm{M_C}}$ or $[100]_{\mathrm{M_C}}$ based on the XRD indexing result. These possible mirror symmetries, however, were not detected by the 1.6-nm diameter probe size. R symmetry can be ruled out directly from the lack of $3m$ symmetry along $[111]_{\mathrm{C}}$. Thus, from local symmetry investigations, significant deviations were observed from the symmetry of all reported structures.

Kisi *et al.* suggests that the observed monoclinic symmetry at the macroscopic scale is not a real phase but a symmetry induced by distortions from a residual stress or piezoelectric response.[15] In this case, the observed monoclinic structure can be considered as a result from the distorted R and T phases. Grinberg *et al.* predicted that the atomic displacements and local distortions varied with the local arrangement of B-site cations in PMN-PT system.[41] Suewattana and coworkers also examined lattice distortions in the PMN system.[42] Locally different atomic displacements have been experimentally determined by Egami, who argued that the local structure of relaxor ferroelectrics is different from the average structure obtained by conventional diffraction methods, such as Rietveld refinement of powder XRD data.[43] Deviations from the reported symmetries at the few nanometers scale are clearly observed in all experimental CBED patterns. Locally distorted structural models are therefore consistent with our observations by use of a 1.6-nm electron probe.

In contrast, the adaptive phase model proposes that the monoclinic symmetry is a result from the twin-related R or T nanodomains.[43–46] We found no evidence of the T and R symmetry at the local scale (1.6-nm probe). Thus the adaptive phase model is not consistent with our experimental observations.

On the other hand, the observed Cm-like symmetry is attained by averaging some regions around 35-nm scale. In other regions, CBED patterns without any symmetry, other than 1-fold rotation, are also observed using the same electron probe size. Hatch *et al.* proposed that averaging over the different volume fraction of domains may lead to different macroscopic symmetries.[47] Thus the symmetry variations observed in the experimental CBED patterns may well reflect the change in local domains and their volume fractions.

The obtained solutions for the Cm-like structure were then confirmed by matching sample orientations by considering the relationship between the monoclinic unit cell axes and the pseudocubic axes for PMN-31%PT. According to the polarization rotation model, the monoclinic unit cell of $\mathrm{M_B}$ is rotated 45° about the c-axis with respect to the pseudocubic c-axis.[1,2,11] The $\mathrm{M_B}$ axes of $a_{\mathrm{M_B}}$ and $b_{\mathrm{M_B}}$ are therefore along the pseudocubic axes of $[\bar{1}\,\bar{1}\,0]_C$ and $[1\,\bar{1}\,0]_C$. The monoclinic c-axis is tilted from the pseudocubic c-axis by β. Figure 9 schematically shows the monoclinic $\mathrm{M_B}$ unit cell with respect to the pseudocubic unit cell for different orientations. In the crystal, the $c_{\mathrm{M_B}}$ can be along any of the three pseudocubic axes of $[001]_{\mathrm{C}}$ [see Fig. 9(a)], $[100]_{\mathrm{C}}$ [see Fig. 9(b)] or $[010]_{\mathrm{C}}$ [see Fig. 9(c)] as confirmed by XRD. For the $[001]_{\mathrm{C}}$, the $\mathrm{M_B}$ structure can be along $\langle 001\rangle$ and $\langle 110\rangle$. For $[011]_{\mathrm{C}}$, the corresponding $\mathrm{M_B}$ zone axes are $\langle 010\rangle_{\mathrm{M_B}}$, (or $\langle 100\rangle_{\mathrm{M_B}}$) and $\langle 112\rangle_{\mathrm{M_B}}$, and for $[111]_{\mathrm{C}}$ they are $\langle 101\rangle_{\mathrm{M_B}}$ and $\langle 011\rangle_{\mathrm{M_B}}$. These relationships are consistent with the solutions of $\mathrm{M_B}$ shown in Fig. 8. Therefore the solutions for the monoclinic Cm ($\mathrm{M_B}$)-like symmetry are supported by not only the CBED simulations but also by the relationships with the crystal orientations.

The presence of the diffraction peaks belonging to different lattice planes in a single crystal XRD pattern suggests that they come from different domains. The large difference in the width of the diffraction peaks between the strong and weak peaks suggests a difference in the average domain size. The size of domains measured by XRD, however, is on the order of hundreds of nanometers as measured by the strong diffraction peaks, which is much larger than the size of nanodomains observed in Fig. 2. On these length scales, it is likely that

XRD averages over multiple domains consisting of the Cm-like symmetry. Whether this averaging leads to the symmetry of M_C, or XRD simply reflects the coexistence of phases, is not clear and requires further clarification.

VI. CONCLUSION

We have investigated the symmetry of PMN-31%PT single crystal from the local scale to the macroscopic scale by using XRD and CBED. The results show that the symmetry of PMN-31%PT is triclinic at a few nm in length scale, and becomes monoclinic Cm-like symmetry at the length scale of a few tens of nm. The macroscopic symmetry determined by XRD suggests multiple domains of different sizes in PMN-31%PT single crystal. Thus the high piezoelectric response of PMN-31%PT single crystal at the MPB region is underlined by a structure that lacks local symmetry, which has an averaged monoclinic symmetry over tens of nanometers in some regions of the crystal. The lack of local symmetry may enhance the polarization switching behavior in this material. The monoclinic Cm-like symmetry provides, in addition, a structural bridge for collective displacements in local regions of tens of nm that is a key to the enhancement of the piezoelectric properties under external electric field. Our result is of importance to show the missing links between the local symmetry and macroscopic symmetry.

ACKNOWLEDGMENTS

The work is supported by DOE BES (Grant No. DEFG02-01ER45923). Electron microscopy was carried out at the Center for Microanalysis of Materials at the Frederick Seitz Materials Research Laboratory of University of Illinois at Urbana-Champaign. We thank Pengdi Han and Jian Tian of H.C Materials (Bolingbrook, IL, USA) for providing PMN-PT single crystals.

---

[*] Corresponding author: jianzuo@illinois.edu

[1] B. Noheda, J. A. Gonzalo, L. E. Cross, R. Guo, S. E. Park, D. E. Cox, and G. Shirane, Phys. Rev. B **61**, 8687 (2000).

[2] B. Noheda, Curr. Opin. Solid State Mater. Sci. **6**, 27 (2002).

[3] S. E. Park and T. R. Shrout, J. Appl. Phys. **82**, 1804 (1997).

[4] S. E. Park and W. Hackenberger, Curr. Opin. Solid State Mater. Sci. **6**, 11 (2002).

[5] M. Davis, J. Electroceram. **19**, 23 (2007).

[6] G. Xu, H. Luo, H. Xu, and Z. Yin, Phys. Rev. B **64**, 020102 (2001).

[7] Z. G. Ye, B. Noheda, M. Dong, D. Cox, and G. Shirane, Phys. Rev. B **64**, 184114 (2001).

[8] B. Noheda, D. E. Cox, G. Shirane, J. Gao, and Z. G. Ye, Phys. Rev. B **66**, 054104 (2002).

[9] A. K. Singh and D. Pandey, Phys. Rev. B **67**, 064102 (2003).

[10] A. K. Singh, D. Pandey, and O. Zaharko, Phys. Rev. B **74**, 024101 (2006).

[11] B. Noheda and D. E. Cox, Phase. Transit. **79**, 5 (2006).

[12] D. Vanderbilt and M. H. Cohen, Phys. Rev. B **63**, 094108 (2001).

[13] M. K. Durbin, J. C. Hicks, S. E. Park, and T. R. Shrout, J. Appl. Phys. **87**, 8159 (2000).

[14] J. K. Lee, J. Y. Yi, K. S. Hong, S. E. Park, and J. Millan, J. Appl. Phys. **91**, 4474 (2002).

[15] E. H. Kisi, R. O. Piltz, J. S. Forrester, and C. J. Howard, J. Phys.: Condens. Matter **15**, 3631 (2003).

[16] D. Viehland, J. Appl. Phys. **88**, 4794 (2000).

[17] H. Wang, J. Zhu, N. Lu, A. A. Bokov, Z. G. Ye, and X. W. Zhang, Appl. Phys. Lett. **89**, 042908 (2006).

[18] H. Wang, J. Zhu, X. W. Zhang, Y. X. Tang, and H. S. Luo, J. Am. Ceram. Soc. **91**, 2382 (2008).

[19] H. Wang, J. Zhu, X. W. Zhang, Y. X. Tang, and H. S. Luo, Appl. Phys. Lett. **92**, 132906 (2008).

[20] J. Tian, P. Han, and D. A. Payne, IEEE Trans. Ultrason. Ferroelectr. Freq. Control **54**, 1895 (2007).

[21] B. F. Buxton, J. A. Eades, J. W. Steeds, and G. M. Rackham, Philos. Trans. R. Soc. London A **281**, 171 (1976).

[22] J. C. H. Spence and J. M. Zuo, *Electron Microdiffraction* (Plenum Press, New York, 1992).

[23] J. A. Eades, *Convergent-Beam Diffraction* (A.R. Liss, New York, 1989).

[24] M. Tanaka, Acta Crystallogr. Sect. A **50**, 261 (1994).

[25] J. P. Morniroli and J. W. Steeds, Ultramicroscopy **45**, 219 (1992).

[26] R. Schierholz, H. Fuess, K. Tsuda, Y. Ogata, M. Terauchi, and R. Theissmann, Phys. Rev. B **78**, 024118 (2008).

[27] R. Schierholz and H. Fuess, Phys. Rev. B **84**, 064122 (2011).

[28] J. M. Zuo, J. C. H. Spence, and R. Hoier, Phys. Rev. Lett. **62**, 547 (1989).

[29] S. P. Singh, A. K. Singh, and D. Pandey, J. Phys.: Condens. Matter **19**, 036217 (2007).

[30] K. H. Kim, D. A. Payne, and J. M. Zuo, Appl. Phys. Lett. **97**, 261910 (2010).

[31] K.-H. Kim and J.-M. Zuo, Ultramicroscopy **124**, 71 (2013).

[32] O. Noblanc, P. Gaucher, and G. Calvarin, J. Appl. Phys. **79**, 4291 (1996).

[33] H. Ohwa, M. Iwata, H. Orihara, N. Yasuda, and Y. Ishibashi, J. Phys. Soc. Jpn. **70**, 3149 (2001).

[34] V. A. Shuvaeva, A. M. Glazer, and D. Zekria, J. Phys.: Condens. Matter **17**, 5709 (2005).

[35] A. Slodczyk, A. Kania, P. Daniel, and A. Ratuszna, J. Phys. D: Appl. Phys. **38**, 2910 (2005).

[36] P. A. Doyle and P. S. Turner, Acta Crystallogr. Sect. A **24**, 390 (1968).

[37] D. M. Bird and Q. A. King, Acta Crystallogr. Sect. A **46**, 202 (1990).

[38] D. Viehland, M. C. Kim, Z. Xu, and J. F. Li, Appl. Phys. Lett. **67**, 2471 (1995).

[39] S. Bhattacharyya, J. R. Jinschek, H. Cao, Y. U. Wang, J. Li, and D. Viehland, Appl. Phys. Lett. **92**, 142904 (2008).

[40] Z. Xu, M. C. Kim, J. F. Li, and D. Viehland, Philos. Mag. **74**, 395 (1996).

[41] I. Grinberg and A. M. Rappe, Phys. Rev. B **70**, 220101(R) (2004).

[42] M. Suewattana and D. J. Singh, Phys. Rev. B **73**, 224105 (2006).

[43] A. G. Khachaturyan, S. M. Shapiro, and S. Semenovskaya, Phys. Rev. B **43**, 10832 (1991).

[44] Y. M. Jin, Y. U. Wang, A. G. Khachaturyan, J. F. Li, and D. Viehland, J. Appl. Phys. **94**, 3629 (2003).

[45] A. G. Khachaturyan, Philos. Mag. **90**, 37 (2010).

[46] Y. U. Wang, Phys. Rev. B **76**, 024108 (2007).

[47] D. M. Hatch, H. T. Stokes, and W. Cao, J. Appl. Phys. **94**, 5220 (2003).